



Title	Diatom records in the Quaternary marine sequences around the Japanese Islands
Author(s)	Koizumi, Itaru; Yamamoto, Hirofumi
Citation	Quaternary international, 397, 436-447 https://doi.org/10.1016/j.quaint.2015.03.043
Issue Date	2016-03-18
Doc URL	http://hdl.handle.net/2115/68358
Rights	©2016 This manuscript version is made available under the CC-BY-NC-ND 4.0 license http://creativecommons.org/licenses/by-nc-nd/4.0/
Rights(URL)	http://creativecommons.org/licenses/by-nc-nd/4.0/
Type	article (author version)
File Information	QUATINT-D-14-00525.pdf



[Instructions for use](#)

Diatom Records in the Quaternary Marine Sequences around the Japanese Islands

Itaru Koizumi^{a,*}, Hirofumi Yamamoto^b

^a Emeritus Professor of Hokkaido University

Atsubetsu-kita 3-5-18-2, Atsubetsu-ku, Sapporo 004-0073, Japan

^b Japan Agency for Marine-Earth Science and Technology (JAMSTEC)

2-15 Natsushima-cho, Yokosuka-city, Kanagawa 237-0061, Japan

* Corresponding author. E-mail addresses: itaru@sci.hokudai.ac.jp (Itaru Koizumi), yamamotoh@jamstec.go.jp (H. Yamamoto).

Keywords: Td' -derived paleo-SSTs (°C), Twt , wavelet analysis, DSDP-ODP, Tohoku Area, Japan Sea

ABSTRACT

Understanding the Quaternary is a key to estimating what the Earth's climate will be like in the future. Such studies demand high-resolution analyses based on the paleoclimatic proxy records of changing the Earth's orbital forcing and solar insolation that affect the climate system. Quaternary diatom biostratigraphy and paleoceanography have been well established based on the Quaternary marine sequences obtained by piston coring and deep-sea drilling around the Japanese Islands. This paper firstly reviews the Quaternary diatom datum levels that are directly tied to magnetic polarity, and then the late Pleistocene and Holocene rhythmic fluctuations in Td' -derived SSTs (°C) which correlate with the Earth's orbital parameters, and finally reveals the large and abrupt climatic changes that have occurred around the Japanese Islands on centennial to millennial time scales.

The main aim is to provide the results of Td' -SSTs (°C) based on the late Pliocene to Pleistocene sequences from three holes obtained by deep-sea drilling (DSDP-ODP). The main difference between Td' and Twt is that Twt gives 0.5 values to Xt (warm transitional taxa). *Thalassiosira oestrupii* is grouped with Xt in Twt but with warm-water species in Td' based on the information of Sancetta and Silvestri (1986),

Koizumi et al. (2004), and Ren et al. (2014). Differences between the *Twt* and *Td'*-SSTs (°C) curves at Hole 436 are unremarkable. The remarkable variations of paleo-temperatures based on *Td'*-SSTs (°C) show four conspicuous episodes which correspond to the two steps noted by Ravelo et al. (2004) and the double precession cycle of the interglacial MIS 11 (Lisiecki and Raymo, 2005). In the Japan Sea, the *Twt* ratio remarkably decreases at 2.6 Ma due to a large increase in cold-water taxa, and indicates the beginning of the glacial age defined as the Pliocene/Pleistocene boundary. Both *Twt* and *Td'*-SSTs (°C) increase at 2.60-2.0 Ma, and coincide with the lithologic change from diatom-bearing clay with few dark-colored layers to fine-grained sediments with distinct dark-light colored cycles. Wavelet analysis of *Td'*-SSTs (°C) at Site 798 indicates a reversed saw-tooth pattern of 48 to 24-kyr periods during 1.2-0.7 Ma, and 24 to 12-kyr periods during 0.7-0 Ma, resulting in a change from longer to shorter cycles. These fluctuations correlate with the Earth's orbital parameters and climatic changes on a millennial time scale.

1. Introduction

Diatom fossils occur more frequently in sediments of the northwest Pacific than other microfossils, and with a greater diversity of species. Diatom biostratigraphy and paleoceanography have been established for the marine Quaternary around the Japanese Islands during the past 10 years (Fig. 1). The Quaternary diatom datum levels (bio-horizons) were directly tied to the magnetic polarity in complete Quaternary marine sequences obtained by the Deep Sea Drilling Project (DSDP) and Ocean Drilling Program (ODP). Within the middle-to-high latitudes, the first occurrence or base (FO) of *Neodenticula seminae* is estimated at 2.7 Ma, the last occurrence or top (LO) of *Neodenticula kamtschatica* at 2.6 Ma, the LO of *Thalassiosira convexa* at 2.3 Ma, the LO of *Thalassiosira zabelinae* at 2.1 Ma, the FO of *Fragilariopsis doliolus* at 2.0 Ma, the LO of *Neodenticula koizumii* at 1.8 Ma, the LO of *Thalassiosira antiqua* at 1.7 Ma, the FO and LO of *Proboscia curvirostris* at 1.6 and 0.3 Ma respectively, the LO of *Actinocyclus oculatus* at 1.0 Ma, and the LO of *Thalassiosira jouseae* at 0.3 Ma (Koizumi, 2009). These datum levels suggest the following evolutionary lineages: (1) from *N. kamtschatica* to *N. koizumii*, (2) from *N. koizumii* to *N. seminae*, (3) from *Fragilariopsis fossilis* to *F. doliolus*, (4) from *Proboscia barboi* to *P. curvirostris*. The

spatial distributions of the appearances and disappearances of diatom species are related to environmental changes and/or to evolutionary processes. The temporal migration of species from their “home-area” to other areas is recognized by delayed first occurrences in those regions and is controlled by the fluctuating frontal boundaries between water-masses (Koizumi, 1986). The disappearance of the species in a given region occurs in response to changing surface-water temperatures (and/or salinities), which are beyond the tolerance limitation of the species.

Paleoceanographic proxies of diatoms have been constructed using statistical methods comparing the spatial distribution of diatom species in the seafloor surface sediments to the primary production, sea-surface temperatures (SSTs) (°C), salinity, and other physical-chemical parameters in modern surface waters. Regression analysis was performed between the ratio of warm- and cold-water diatom species (revised diatom temperature ratio, Td' ratio) in 123 surface sediments around the Japanese Islands and annual SSTs (°C) at the core sites (Koizumi, 2008; Table 1). Td' -derived annual paleo-SSTs (°C) agree with the $\delta^{18}\text{O}$ of benthic foraminiferal tests and Uk'_{37} -derived summer paleo-SSTs (°C) at sites off central Japan. Td' -SSTs (°C) fluctuate on centennial to millennial timescales, indicating a strong and regular flow of the Kuroshio Current and Tsushima Warm Current (TWC) during the Holocene epoch after 12 ka (Koizumi and Yamamoto, 2010, 2011). The Td' -SSTs (°C) in the Tohoku Area off the northeast part of Honshu Island are generally higher than in the Japan Sea despite lower Td' values because the warm-water species *Fragilariopsis doliolus* is abundant only in the TWC of the Japan Sea. Those fluctuations are synchronous with abrupt climate events reported from the different paleoclimatic proxy records in many regions of the Northern Hemisphere (Koizumi and Sakamoto, 2010; Koizumi and Yamamoto, 2011).

The Td' -SSTs (°C) decrease during the Younger Dryas (YD) due to a weakening of both the Kuroshio and TWC (Koizumi, 2008). The average SSTs (°C) in the YD are 7-9 °C lower than the present-day values in the Tohoku Area, and 6-9 °C lower than those in the Japan Sea. The early Holocene (11.6-8.2 ka) is a transitional period characterized by a long-term increasing trend of temperatures punctuated by several cooling events, while the middle Holocene (8.2-3.3 ka) coincides with the Holocene hypsithermal period and is 1-2 °C warmer than the earlier and later parts of the Holocene. The late Holocene (3.3-0 ka) neo-glacial period is marked by a generally

decreasing trend of the SSTs (°C), reflecting the decreased solar insolation in the Northern Hemisphere summer (Koizumi and Sakamoto, 2010).

The middle Holocene warm period in the Tohoku Area is marked by the anti-phased SST relationship with decreasing abundances of the warm-water diatom species *F. doliolus* (Barron and Anderson, 2010) and the alkenone-derived (Yamamoto et al., 2004; Isono et al., 2009) SSTs (°C) in coastal northern California. The anti-phase SST variations between east-to-west margins of the mid-latitude North Pacific Ocean are similar to the behaviors of the El Niño-Southern Oscillation (ENSO). The anti-phase SST variations also correspond to the patterns seen in the modern Pacific-Decadal Oscillation (PDO), where cooler SSTs in the central northwest Pacific Ocean contrast with warmer SSTs in the eastern North Pacific Ocean and eastern equatorial Pacific Ocean during periods of positive PDO (Isono et al., 2009; Barron and Anderson, 2010).

The Pliocene/Pleistocene boundary was changed to 2.58 Ma at the top of magnetic polarity C2An (Gauss) chron by the International Union for Quaternary Research (INQUA) and International Commission on Stratigraphy (ICS) (Head et al., 2008).

The purpose of this paper is to define the paleoclimatic and paleoceanographic events based on the original database for Td' -SSTs (°C) and diatom assemblages in a series of excellent biosiliceous sequences after 3.6 Ma at DSDP Site 436 in the Tohoku Area off the northeast Japan, and after 3.3 Ma at ODP Hole 797B and after 1.3 Ma at Holes 798A and 798C in the Japan Sea (Fig. 1).

2. Background

The onset of significant Northern Hemisphere Glaciation (NHG) at ~2.7 Ma occurred within the context of progressive Cenozoic cooling (Koizumi, 1985; Barron, 1998; Shimada et al., 2009), and also a gradual increase in the mean global ice volume began in the interval of 3.6 Ma to 2.4 Ma (Ravelo et al., 2004) based on deep-sea drilling cores. Prior to the onset of NHG, the Pliocene warm period (5-3 Ma) was widely studied as an analogue of a future global climate warmer than today.

On the other hand, diatom records mainly in piston cores have shown oscillations between warm and cold Pleistocene intervals and have recorded glacial-interglacial

cycles twice over 150 ka. Diatom associations and Td' -SSTs (°C) imply that paleohydrography around the Japanese Islands has corresponded to environmental changes such as Milankovitch cycles, Dansgaard-Oeschger cycles and/or Bond cycles on an orbital timescale between warm and cold intervals (Koizumi and Sakamoto, 2010; Koizumi and Yamamoto, 2010, 2011).

2.1. Paleotemperature Estimates in the late Pliocene to early Pleistocene

The U.S. Geological Survey organized the PRISM (Pliocene Research, Interpretation, and Synoptic Mapping) Project in 1990 (Cronin and Dowsett, 1991). In the PRISM Project, Barron (1992) proposed the use of the Twt ratio to interpret the Pliocene paleoclimatic changes in the region of DSDP Site 580 in the northwest Pacific. In the equation $Twt=(Xw+0.5Xt)/(Xc+Xt+Xw)$, Xw is the total number of subtropical to tropical (warm-water) taxa. Xt is the total number of warm transitional taxa (*Thalassionema nitzschioides*, *Thalassiosira oestrupii*, and *Coscinodiscus radiatus*) and Xc is the total number of subarctic to arctic (cold-water) taxa. Xw and Xc include extinct Pliocene taxa, for instance *Fragilariopsis fossilis*, *F. reinholdii*, *Nitzschia jouseae* and *Thalassiosira convexa* as Xw , and *Neodenticula kamtschatica* and *N. koizumii* as Xc .

The Twt ratio in this paper constitutes the associated taxa, which the Td' ratio (Table 1; Koizumi, 2008) introduced and includes such extinct Pliocene taxa, in addition to those Barron (1992) adopted, as *Nitzschia miocenica*, *Rhizosolenia praebergonii*, *Thalassiosira miocenica*, and *T. praeconvexa* as Xw , and *Actinocyclus oculatus*, *Proboscia curvirostris*, and *Thalassiosira nidulus* as Xc . These taxa are considered to closely correspond to their descendants based on their morphology, paleogeographic distribution, and ecological requirements. *T. oestrupii* is converted from warm-water species in Td' to Xt in Twt (Table 2) because *T. oestrupii* prefers a relatively cooler environment (Ren et al., 2014). However, Td' -derived SST (°C) values still substitute substantially for the paleotemperatures (°C).

2.2. Climatic Changes based on Td' -derived SSTs (°C) in the late Pleistocene

Diatom records in the Tohoku Area have shown glacial-interglacial cycles twice

over the past 150,000 years, which corresponds to the environmental changes on an orbital timescale (Koizumi and Yamamoto, 2010). The high Td' -derived SSTs ($^{\circ}\text{C}$) recognized in middle MIS 5e and 1 of the interglacial phase correlate among the cores. Td' -SSTs ($^{\circ}\text{C}$) in MIS 5e are $\sim 5^{\circ}\text{C}$ higher than modern values from near-shore cores, but in the offshore cores the differences are only up to $\sim 1.5^{\circ}\text{C}$. On the other hand, the remarkable decline of Td' -SSTs ($^{\circ}\text{C}$), recognized in the MIS event 6.0 at the MIS 6/5 boundary and event 5.2 in MIS 5b, correspond to the ages of Heinrich events 1-6 in the northern North Atlantic (Heinrich, 1988).

Fluctuations in Td' -SST ($^{\circ}\text{C}$) over 150,000 years show a reversed saw-tooth pattern with the duration of about 30-kyr in the southern area, but a shape of a saw-tooth at about 40-kyr periods in the northern area (Koizumi and Yamamoto, 2010). According to the suggestion by modern oceanographic observations and modeling, the winter Aleutian Low develop strong westerly below along the latitude of about 35°N (Ishi and Hanawa, 2005). Correspondingly, the Sverdrup transports as western boundary currents cause both the increase (decrease) in the flow of the Kuroshio Current and the decrease (increase) of the Oyashio Current simultaneously. The Td' -SSTs ($^{\circ}\text{C}$) records fluctuate at 118-kyr, 60-kyr, 30-kyr, and 23-kyr periods. The lower frequencies in 96 to 112-kyr and 7.2 to 12.8-kyr periods correspond to Bond cycles (Alley, 1998). A periodicity of a ~ 32 -kyr period corresponds to the periodicity of the long-term orbital-scale ENSO (Clement et al., 1999). The shorter period of 1.4 to 2.1-kyr corresponds to Heinrich events (Heinrich, 1988), Dansgaard-Oeschger cycles (Alley, 1998), the fluctuations of residual $\Delta^{14}\text{C}$ record with variance on ~ 2 -kyr cycle (Stuiver et al., 1991), and the ~ 2 -kyr cycle in the variability of ENSO activity (Moy et al., 2002).

Td' -SSTs ($^{\circ}\text{C}$) over 160,000 years in the southern area of the Japan Sea fluctuated at a 48-kyr period between 160-90 ka and 45-0 ka due to orbital-obliquity (tilt) cycles, and at a 23-kyr period, orbital precession cycles, during the 140-100 ka interval (Koizumi and Yamamoto, 2011). The predominant periodicities of 2-kyr and 4-kyr periods occurred at intervals of 20 and 40 ka. However, the SSTs ($^{\circ}\text{C}$) of stadial phases in the northern area could not be reconstructed because of very few marker diatom species. Diatom abundances in the Subarctic Boundary are almost negligible except during MIS 5e, 2, and 1.

2.3. Oceanic Primary Production in the late Pleistocene

The oceanic diatom abundances in the northern area are twice to three times as high as those in the southern area in the Tohoku Area off the northeast Japan. The fluctuations of abundances in the northern area show a reversed saw-tooth pattern from lower abundance to higher values at about 40-kyr periods. This pattern is opposite to a saw-tooth shape in the Td' -derived SSTs ($^{\circ}\text{C}$) because primary production of oceanic diatoms from interglacial to glacial periods due to the orbital forcing should be promoted by vertical and lateral mixing between cold and warm waters by glacio-eustatic sea level changing closely related to the Aleutian Low (Goes et al., 2001).

3. Material and method of study

3.1. Material

We used the original database from DSDP Site 436 (Koizumi and Sakamoto, 2012; Table 4 appendix) in the Tohoku Area off northeast Japan, and ODP Holes 797B (Koizumi, 1992; Koizumi and Ikeda, 1997; Table 5 appendix), Holes 798 A and C (Table 6 appendix) in the Japan Sea (Fig. 1). The chronostratigraphic framework (sub-bottom depth-mcd versus sediment age-Ma) in the three cores is based on the paleomagnetic data (Shipboard Scientific Party, 1990a; Hamano et al., 1992), diatom datum levels (Koizumi, 1992; Koizumi and Sakamoto, 2012) and tepthrostratigraphy (Koizumi and Ikeda, 1997; Aoki and Sakamoto, 2003) as shown in Table 3 and Fig. 2.

Site 436 is located near the crest of outer swell seaward of the Japan Trench ($39^{\circ}55.96'\text{N}$, $145^{\circ}33.4'\text{E}$; water-depth 5240 m). The sediments consist of olive gray vitric diatomaceous silty clay in the upper 245 mcd of the Plio-Pleistocene sequence. 26 samples obtained with the average sampling interval is ~ 7.23 m corresponding to 0.14 m.y. The Pliocene/Pleistocene boundary at ~ 2.6 Ma is defined by the last common occurrence of *N. kamtschatica* between 135.0 and 122.4 mcd (Table 4 appendix). The sediment accumulation rates are subdivided into three parts (Fig. 2): (1) 50.56 m/m.y. through the late Pliocene to early Pleistocene (3.72 to 1.24 Ma), (2) decrease to 27.13 m/m.y. between 1.24 and 0.3 Ma, and (3) increase to 123.67 m/m.y.

Hole 797B is located in the southwestern Yamato Basin of south-central Japan Sea (38°10.27'N, 134°8.93'E; water-depth 2862m). Thin interbeds of dark, indistinctly laminated clay and silty clay which contain pyrite, diatoms and organic matter, alternate with light-colored, well-bioturbated clay and silty clay in the upper sequence of the C2n (Olduvai) chron at the sub-bottom depth ~82 mcd. The sequence between 120–82 mcd of uppermost Pliocene to lowest Pleistocene (2.8–1.9 Ma) consists of light gray, moderately bioturbated, diatom-bearing ashy clay and silty clay with few dark-colored layers. The sequence between 170–120 mcd (3.2–2.8 Ma) is characterized by a significant increase of diatoms and the absence of color bands (Table 5 appendix; Fig. 5). We analyzed 38 samples obtained with the average sampling interval is ~4.05 m corresponding to 0.097 m.y. without the basal interval of 61.29–125.47 m (Fig. 2). The paleomagnetic polarity pattern is not always obvious in the sediments from the Japan Sea, because the intensity of magnetization of the sediments is quite weak and polarity intervals are disturbed by reversed polarity intervals. Despite the uncertainties in the polarity pattern, a reasonable correlation with the Geomagnetic Reference Time Scale for the late Pliocene-Quaternary has been defined (Table 3; Shipboard Scientific Party, 1990a; Hamano et al., 1992). The sediment accumulation rates are also subdivided into three parts: (1) inordinately high 237.5 m/m.y. between 3.21 and 3.01 Ma, (2) 33.77 m/m.y. through 3.01 to 1.00 Ma, and (3) 57.52 m/m.y. after 1.00 Ma (Fig. 2).

Holes 798A (37.04°N, 134.80°E; water-depth 903 m) and 798C (37.04°N, 134.08°E; water-depth 900 m) are located on the top of Oki Ridge in the southeastern portion of the Yamato Basin. The uppermost sediments of Hole 798C (0.41-3.40 mcd) were added to the uppermost part of the Pleistocene section (3.67-124.3 mcd) of Hole 798A. The Quaternary sequence is composed of mainly clay, diatomaceous clay and diatom ooze with calcareous inter-beds. The dark, laminated organic-rich diatomaceous sediments and the light-colored clay-rich, bioturbated sediments alternate on a centimeter- to decimeter-scale (Shipboard Scientific Party, 1990b). We analyzed 123 samples obtained with the average sampling interval is 1.00 m corresponding to 10.37 kyr throughout the sequence (Table 6 appendix; Fig. 2). The chronostratigraphic framework was decided by the last occurrences at 0.3 Ma of *P. curvirostris* between 44.9 and 38.8 mcd, and the magnetic polarity of C1n (Brunhes) chron and C1r (Jaramillo) chron (Table 3). Site 798 has a constant sedimentation rate

of 96.66 m/m.y. with a break at 84.5 mcd (0.86 Ma) (Fig. 2).

3.2. Methods

We chose wavelet analysis to evaluate the time series of the values in the band ration Td' -derived annual paleo-SSTs (°C) at century-millennial timescales in Holes 798A and C. The Fourier spectral analysis is the most common tool to analyze the frequency pattern of a signal. Short-time Fourier transform uses a sliding window to fined spectrogram, which gives the information of both time and frequency. However, the length of window limits the resolution in frequency. The limited ability of classical Fourier spectral analysis to detect a 1500-year climate cycles (e.g. Bond et al., 2001) that evolves through time were discussed by Debret et al. (2007). The wavelet transform, contrary to the Fourier transform, is used to decompose a signal into a sum of small wave functions of a finite length that are highly localized in time, for different exploratory scales.

The wavelet software provided by Torrence and Compo (1998) are available at URL: <http://paos.colorado.edu/research/wavelet/>. N=1283 by statistical complement. The time series were padded with zero, and parameters \times interval=0.001, start scale=4, scale width=0.001 and mother wavelet=Morlet. Significance levels were set at 10 %, and a red-noise (autoregressive lag 1) background was estimated from the alpha parameter described in Torrence and Compo (1998).

Blanks /gaps in the data were filled up/interpolated using a cubic spline interpolant (passes exactly through each data point).

Wavelet transform is a band-pass filter which consists of convoluting the signal with scaled and translated forms of a highly time-localized wave function (the filter), so-called “mother wavelet”. We chose the Morlet wavelet (a gaussian-modulated sine wave) for continuous wavelet transform:

$$\psi_0(\eta) = \pi^{-1/4} e^{i\omega_0\eta} e^{-\eta^2/2}$$

where ψ_0 is the wavelet value at non-dimensional time η , η is a dimensionless time parameter and ω_0 is the wavenumber that defines the basic resolution of the mother wavelet. A wavenumber of 6 was used (Farge, 1992).

To avoid edge effects and spectral leakage that are produced by the finite length of

the time series, the series were zero-padded to twice the data length. However, zero-padding causes the lowest frequencies near the edges of the spectrum to be underestimated as more zeros enter the series. The area delineating this region is known as the cone of influence ((Debret et al., 2007).

The Cone of influence (COI) is the region of the wavelet spectrum in which edge effects become important and is defined here as the e-folding time for the autocorrelation of wavelet power at each scale (Table 1 of Torrence and Compo, 1998). For concreteness, the width of a wavelet function is defined here as the e-folding time of the wavelet amplitude. This e-folding time is chosen so that the wavelet power for a discontinuity at the edge drops by a factor e^{-2} and ensures that the edge effects are negligible beyond this point.

The size of the COI at each scale also gives a measure of the decorrelation time for a single spike in the time series. By comparing the width of a peak in the wavelet power spectrum with this decorrelation time, one can distinguish between a spike in the data (possibly due to random noise) and a harmonic component at the equivalent Fourier frequency.

For all local wavelet spectra, monte carlo simulation was used to assess the statistical significance of peaks.

4. Tohoku Area off the Northeast Japan

4.1. Hydrographic Condition

The ocean waters off the east coast of the Japanese Islands have four different surface water regions (Fig. 3): (1) the Subtropical Gyre with the Kuroshio and Kuroshio Extension flowing eastward, (2) the Mixed Water Region offshore between 35° and 40° N, (3) the Transition Domain in the eastern than 150° E with increasing flows eastward under the influences of Kuroshio and Oyashio waters, and (4) the Subarctic Gyre (Masujima et al., 2003). The Oyashio is the western boundary current of the western Subarctic Gyre in the North Pacific. The hydrographic complexities in the Mixed Water Region cause local upwelling due to the isopycnal mixing between the subarctic and subtropical water masses, different velocities and vertically different salinities, and thus cause high phytoplankton productivity.

4.2. Diatom Assemblages in the Plio-Pleistocene Sequence

The difference between the *Twt* and *Td'*-SST (°C) curve is unremarkable off the northeast Japan, but the *Twt* ratio remarkably drops due to the predominance of cold-water extinct species *N. kamtschatica* at 3.6-3.2 Ma and *N. koizumii* at 2.2 Ma, while the *Td'*-SST (°C) curve does not (Fig. 4).

The remarkable variations of paleo-temperatures based on *Td'*-SSTs (°C) at DSDP Site 436 show four conspicuous episodes: (1) decreasing from 18.5 °C at 3.5 Ma to 15.1 °C at 2.65 Ma, when approximately coincide with the lithologic change from oxidized clay to anoxic biosiliceous clay and indicate the onset of significant NHG at the first step (between 3.0 and 2.5 Ma) indicated by Ravelo et al. (2004), (2) afterwards increasing to 21.7 °C at 2.1 Ma, and then (3) decreasing from 21.7 °C at 2.1 Ma to 10.1 °C at 1.4 Ma, which occurred well after the onset of significant NHG at the second step (between 2.0 and 1.5 Ma) of Ravelo et al. (2004), (4) slight fluctuations occurring around space 0.3 Ma and corresponding to the Mid-Brunhes Event (Jansen et al., 1986) were forced by the orbital eccentricity cycle. Recent research has focused on MIS 11 (between 0.42 and 0.40 Ma) as a possible analog for the present interglacial, because MIS 11 spans two precession cycles with $\delta^{18}\text{O}$ values below 3.6 ‰ for 20 kyr (Lisiecki and Raymo, 2005). After this event, the climatic trend changes towards more glacial conditions in the Northern Hemisphere.

5. Japan Sea

5.1. Hydrographic Condition

The Japan Sea is a semi-enclosed marginal sea located on the eastern end of the Asian continent with its eastern margin bounded by the Japanese Island Arc (Fig. 3). Water exchange between the Japan Sea and adjacent seas have mainly occurred through four narrow and shallow straits, the Tsushima Strait (TSS) connecting to the East China Sea, the Tsugaru Strait (TGS) to the Pacific Ocean, and the Soya Strait (SS) and Mamiya Strait (MS) to the Okhotsk Sea. It has responded to eustatic sea-level fluctuations influenced by global climatic change during the late Quaternary, especially the glacial-interglacial period. Four main currents, the Tsushima Warm Current (TWC), the East Korean Warm Current (EKWC), the Liman Current (LC) and the North Korean

Cold Current (NKCC), exist in the Japan Sea (Senjyu, 1999). The TWC, which is a branch of the Kuroshio, meanders in the southeastern part and diverges again into two branches in the western area of the Tsugaru Strait.

5.2. Late Pliocene-Pleistocene Sequences

The period from the latest Pliocene to Pleistocene is characterized by a significant decrease in diatomaceous sedimentation, an increase in volcanic-ash production and terrigenous input, and oscillating climate. The last occurrences at 2.00 Ma of *N. koizumii* between 90.49 and 84.49 mcd and at 0.3 Ma of *P. curvirostris* between 18.45 and 12.69 mcd were confirmed by comparing with the paleomagnetic time scale (Table 3).

Low frequency and high amplitude fluctuations of both *Twt* and *Td'*-SSTs (°C) occur between 3.2 and 3.0 Ma, when *Twt* gradually increases due to the remarkable decrease of cold-water taxa including extinct *N. kamtschatica* and *N. koizumii* (Fig. 5). After then, the *Twt* ratio remarkably decreases at 2.6 Ma due to a large increase of cold-water taxa, and indicates the beginning of the glacial age defined as the Pliocene and Pleistocene boundary (Head et al., 2008). Both *Twt* and *Td'*-SSTs (°C) increase from 2.6 Ma to 2.0 Ma due to a large decrease of cold-water taxa. This time level approximately coincides with the lithologic change from diatom-bearing ashy clay and silty clay with few dark-colored layers to fine-grained sediments with distinct dark-light colored cycles (Shipboard Scientific Party, 1990a).

Diatom abundance decreased at the time when the Japan Sea was isolated from surrounding seas due to the drop of eustatic sea-level during the glacial to stadial phase, especially causing dissolution and/or low diatom counts in the northern area (Koizumi and Yamamoto, 2011).

5.3. Pleistocene Sequence

Diatom abundances are higher with sharp and short-term fluctuations during four intervals: 1.05-0.95 Ma, 0.68-0.62 Ma, 0.55-0.47 Ma, and 0.12-0.03 Ma (Fig. 6). The sublittoral taxa increased at both 1.3-1.2 and 0.85-0.75 Ma and are composed of *Paralia sulcata*, *Actinoptychus senarius*, *Stephanopyxis turris*, and *Diploneis* spp., but

species composition changed into *Cyclotella striata* and *P. sulcata* at 0.1 Ma.

The Td' -SSTs ($^{\circ}\text{C}$) remarkably decrease from 16°C to 7°C at 1.17 Ma due to increases of the cold-water species *Neodenticula seminae*, and then at 0.66 Ma from 13°C to 8°C due to increases of the cold-water species *Actinocyclus curvatulus*. Those time levels are just after the increase of the warm-water species *Thalassiosira oestrupii* at 1.19 Ma and 0.68 Ma. The changing times from warm-water to cold-water phase are correlated to MIS 37-36 and MIS 17-16 of the LR04 benthic $\delta^{18}\text{O}$ stack (Lisiecki and Raymo, 2005). Around magnetic polarity C1r.1n (Jaramillo) subchron, relative abundances (3-21 %) of cold-water taxa including *N. seminae* display marked fluctuations within a short time interval. The relative abundances of cold-water taxa are also correlated to MIS 30-26 (around the top of the Jaramillo subchron) of the LR04 stack. The pronounced occurrences of warm-water taxa including both *Fragilariopsis doliolus* and *T. oestrupii* at 0.16-0.13 Ma may have been caused by conditions 4°C warmer than the present-day 16°C , which is correlated to MIS 5, Termination II.

Wavelet analysis for Td' -SSTs ($^{\circ}\text{C}$) indicates a reversed saw-tooth pattern, which is characteristic in warm-water mass (Koizumi and Yamamoto, 2010), of 48 to 24-kyr periods during 1.2-0.7 Ma, and 24 to 12-kyr periods during 0.7-0 Ma, resulting in a change from longer cycles to shorter cycles (Fig. 7). Those periods indicate as black line (variance) is fully distinguished from red-noise showing by the dashed line (Fig. 7c). Variability of 48 to 24-kyr periods correspondence to the orbital obliquity (tilt) and precession cycles, and also 24 to 12-kyr periods to the precession. Variability of 130-kyr periods, corresponding to orbital eccentricity, is recognized around 1.1 to 0.8 Ma. The transitional change in dominance from obliquity to precession with minor effect of eccentricity, suggesting local ocean-related climate influences around 0.8-0.7 Ma.

6. Conclusions

Deep-sea drilling around the Japanese Islands has provided excellent Quaternary marine materials for the study of diatom biostratigraphy and paleoceanography. Results from Site 436 in the Tohoku Area off the northeast Japan have shown remarkable variations of Td' -SSTs ($^{\circ}\text{C}$) at four conspicuous episodes: (1) decreasing from 18.5°C

at 3.5 Ma to 15.1 °C at 2.65 Ma, (2) afterwards increasing to 21.7 °C at 2.1 Ma, (3) decreasing from 21.7 °C to 10.1 °C at 1.4 Ma, and (4) slightly fluctuating around 0.3 Ma.

In the Japan Sea, the *Twt* ratio of Hole 797B remarkably decreases at 2.6 Ma due to large increases of cold-water taxa. Both *Twt* and *Td'*-SSTs (°C) increase from 2.6 Ma to 2.0 Ma due to a large decrease of cold-water taxa. Diatom abundances are higher with sharp and short-term fluctuating during four intervals: 1.05-0.95 Ma, 0.68-0.62 Ma, 0.55-0.47 Ma, and 0.16-0.03 Ma. The change from warm-water taxa to cold-water taxa at both 1.19-1.17 Ma and 0.68-0.66 Ma is correlated with MIS 37-36 and MIS 17-16 of the LR04 benthic $\delta^{18}\text{O}$ stack respectively (Lisiecki and Raymo, 2005). Remarkable fluctuation of cold-water taxa around magnetic polarity C1r.1n subchron is also correlated to MIS 30-26. The pronounced occurrences of warm-water taxa at 0.16-0.13 Ma is correlated to MIS 5 (Termination II), but a pronounced peak of warm-water taxa was not recognized at MIS 11 (Termination V). The *Td'*-SSTs (°C) at Site 798 changed from longer cycles, corresponding to the orbital eccentricity and obliquity (tilt) to shorter cycles of the obliquity and precession around 0.8-0.7 Ma in the middle Pleistocene.

Paleoceanographic analysis should be performed based on diatoms also because they are the most diverse and abundant microfossil group in the region.

Acknowledgements

We wish to thank Prof. Richard Jordan of the Yamagata University for his critical reviews and for improvements of English of the draft. We acknowledge with special thanks to Dr. John A. Barron of the USGS at Menlo Park and anony for reviewing critically and suggestions for improving the manuscript better. We also thank Editors, Drs. Norm Catto and Yoshiki Saito for their reviews and editorial work.

References

- Alley, R.B., 1998. Icing the North Atlantic. *Nature* 392, 335-337.
- Aoki, K., Sakamoto, T., 2003. Late Quaternary tephrostratigraphy of the sediments from the Japan Trench forearc, Holes 1150A and 1151C. In: Suyehiro, K., Sacks,

- I.S., Acton, G.D., Oda, M. (eds.) Proc. ODP, Sci. Results, vol. 186, 1-22 (Online).
Available from: http://www-odp.tamu.edu/publications/186_SR/116/116.htm.
- Barron, J.A., 1992. Pliocene paleoclimatic interpretation of DSDP Site 580 (NW Pacific) using diatoms. *Marine Micropaleontology* 29, 23-44.
- Barron, J.A., 1998. Late Neogene changes in diatom sedimentation in the North Pacific. *Journal of Asian Earth Sciences* 16, 85-95.
- Barron, J.A., Anderson, L., 2010. Enhanced late Holocene ENSO/PDO expression along the margins of the eastern North Pacific. *Quaternary International* 235, 3-12.
- Beaufort, L., de Garidel-Thoron, T., Mix, A.C., Pisias, N.G., 2001. ENSO-like forcing on oceanic primary production during the late Pleistocene. *Science* 293, 2440-2444.
- Bond, G.G., Kromer, B., Beer, J., Muscheler, R., Evans, M., Showers, W., Hoffmann, S., Lotti-Bond, R., Hajdas, I., and Bonani, G., 2001. Persistent solar influence on Northern Atlantic climate during the Holocene. *Science* 294, 2130-2136.
- Clement, A.C., Seager, R., Cane, M.A., 1999. Orbital controls on the El Niño/Southern Oscillation and the tropical climate. *Paleoceanography* 14, 441-456.
- Cronin, T.M., Dowsett, H.J., 1991. Pliocene Climate. *Quaternary Science Review* 10, 1-296.
- Debret, M., Bout-Roumazielles, V., Grousset, F., Desmet, M., McManus, J.F., Massei, N., Sebag, D., Petit, J.-R., Copard, Y., Trentesaux, A., 2007. The origin of the 1500-year climate cycles in Holocene North-Atlantic records. *Clim. Past* 3, 569-575.
- Farge, M., 1992. Wavelet transforms and their applications to turbulence. *Ann. Rev. Fluid Mech.*, 24, 395-457.
- Goes, J.I., Gomes, H. do R., Limsakul, A., Balch, W.M., Saino, T., 2001. El Niño related interannual variations in biological production in the North Pacific as evidenced by satellite and ship data. *Progress in Oceanography* 49, 211-225.
- Hamano, Y., Krumsiek, K.A.O., Vigliotti, L., Wipperfurth, J.J.M., 1992. Pliocene-Pleistocene magnetostratigraphy of sediment cores from the Japan Sea. In: Tamaki, K., Suyehiro, K., Allan, J., McWilliams, M., et al. (eds.) *Proceedings of the Ocean Drilling Program, Scientific Results, 127/128, Pt. 2*. College Station, TX: Ocean Drilling Program, 969-982.
- Head, M.J., Gibbard, P., Sahar, A., 2008. The Quaternary: Its character and definition. *Episodes* 31, 234-238.

- Heinrich, H., 1988. Origin and consequences of cyclic ice rafting in the Northeast Atlantic Ocean during the past 130,000 years. *Quaternary Research* 29, 142-152.
- Ishi, Y., Hanawa, K., 2005. Large-scale variabilities of wintertime wind stress curl field in the North Pacific and their relation to atmospheric teleconnection patterns. *Geophysical Research Letters* 32, L10607, doi:10.1029/2004GL022330.
- Isono, D., Yamamoto, M., Irino, T., Oba, T., Murayama, M., Nakamura, T., Kawahata, H., 2009. The 1500-year climate oscillation in the midlatitude North Pacific during the Holocene. *Geology* 37, 591-594.
- Jansen, J.H.F., Kuijpers, A., Troelstra, S.R., 1986. A mid-Brunhes climatic event: Long-term changes in global atmosphere and ocean circulation. *Science* 232, 619-622.
- Koizumi, I., 1985. Late Neogene paleoceanography in the western North Pacific. In: Heath, G.R., Burckle, L.H., et al. (eds.) *Initi. Rep. DSDP, 86, 781-785*, Washington: U.S. Govt. Printing Office.
- Koizumi, I., 1986. Pliocene and Pleistocene diatom datum levels related with paleoceanography in the northwest Pacific. *Marine Micropaleontology* 10, 309-325.
- Koizumi, I., 1992. Diatom biostratigraphy of the Japan Sea: Leg 127. In: Pisciotto, K.A., Ingle, J.C., Jr., von Breyman, M. T., Barron, J., et al. (eds.) *Proc. ODP, Sci. Res., 127/128, Pt. 1, 249-289*, College Station, TX: Ocean Drilling Program.
- Koizumi, I., 2008. Diatom-derived SSTs (*Td'*ratio) indicate warm seas off Japan during the middle Holocene (8.2-3.3 ka BP). *Marine Micropaleontology* 69, 263-281.
- Koizumi, I., 2009. Diatom biostratigraphy and chronology during the Quaternary. *Digital Book Progress in Quaternary Research in Japan*, 1-15, Tokyo, Japan Association for Quaternary Research (in Japanese with English abstract).
- Koizumi, I., 2013. Pacific. In: Elias, S.A. (ed.) *The Encyclopedia of Quaternary Science*, vol. 1, pp. 571-587. Amsterdam: Elsevier.
- Koizumi, I., Ikeda, A., 1997. The Plio-Pleistocene diatom record from ODP Site 797 of the Japan Sea. In: Naiwen, W., Remane, J. (eds.) *Pro. 30th Inter. Geol. Congress*, vol. 11, 213-230, Utrecht: VSP, International Sci. Publishers.
- Koizumi, I., Sakamoto, T., 2003. Paleoceanography off Sanriku, northeast Japan, based on diatom flora. In: Suyehiro, K., Sacks, I.S., Acton, G.D., Oda, M. (eds.) *Proc. ODP, Sci. Results*, vol. 186, 1-21(Online). Available from:

- http://www.odp.tamu.edu/publications/186_SR/110/110.htm.
- Koizumi, I., Sakamoto, T., 2010. Synchronous Td'-derived SSTs (°C) off Japan with climatic events in the northern hemisphere. *Journal of Geography* 119, 489-509 (in Japanese with English abstract).
- Koizumi, I., Sakamoto, T., 2012. Allochthonous diatoms in DSDP Site 436 on the abyssal floor off northeast Japan. *JAMSTEC Report of Research and Development* 14, 27-38.
- Koizumi I., Yamamoto, H., 2010. Paleoceanographic evolution of North Pacific surface water off Japan during the past 150,000 years. *Marine Micropaleontology* 74, 108-118.
- Koizumi, I., Yamamoto, H., 2011. Oceanographic variations over the last 150,000 years in the Japan Sea and synchronous Holocene with the North Hemisphere. *Journal of Asian Earth Sciences* 40, 1203-123.
- Koizumi, I., Irino, T., Oba, T., 2004. Paleoceanography during the last 150 kyr off central Japan based on diatom floras. *Marine Micropaleontology* 53, 293-365.
- Koizumi, I., Tada, R., Narita, H., Irino, T., Aramaki, T., Oba, T., Yamamoto, H., 2006. Paleoceanographic history around the Tsugaru Strait between the Japan Sea and the Northwest Pacific Ocean since 30 cal kyr BP. *Palaeogeography, Palaeoclimatology, Palaeoecology* 232, 36-52.
- Lisiecki, L.E., Raymo, M.E., 2005. A Pliocene-Pleistocene stack of 57 globally distributed benthic $\delta^{18}\text{O}$ records. *Paleoceanography* 20, PA1003, doi:10.1029/2004PA001071.
- Masujima, M., Yasuda, I., Hiroe, Y., Watanabe, T., 2003. Transport of Oyashio Water across the Subarctic Front into the Mixed Water Region and formation of NPIW. *Journal of Oceanography* 59, 855-869.
- Moy, C.M., Seltzer, G.O., Rodbell, D.T., Anderson, D.M., 2002. Variability of El Niño/Southern Oscillation activity at millennial timescales during the Holocene epoch. *Nature* 420, 162-165.
- Ravelo, A.C., Andreasen, D.H., Lyle, M., Lyle, A.O., Mara, M.W., 2004. Regional climate shifts caused by gradual global cooling in the Pliocene epoch. *Nature* 429, 263-267.
- Ren, J., Gersonde, R., Esper, O., Sancetta, C., 2014. Diatom distributions in northern North Pacific surface sediments and their relationship to modern environmental

- variables. *Palaeogeography, Palaeoclimatology, Palaeoecology* 402, 81-103.
- Sancetta, C.A., Silvestri, S.M., 1986. Pliocene-Pleistocene evolution of the North Pacific ocean-atmosphere system, interpreted from fossil diatoms. *Paleoceanography* 1, 163-180.
- Senjyu, T., 1999. The Japan Sea Intermediate Water; its characteristics and circulation. *Journal of Oceanography* 55, 111-122.
- Shimada, C., Sato, T., Yamasaki, M., Hasegawa, S., Tanaka, Y., 2009. Drastic change in the late Pliocene subarctic Pacific diatom community associated with the onset of the Northern Hemisphere Glaciation. *Palaeogeography, Palaeoclimatology, Palaeoecology* 279, 207-215.
- Shipboard Scientific Party, 1990a. Site 797. In: Tamaki, K., Pisciotta, J., Allan, J., et al. (eds.) *Proceedings of the Ocean Drilling Program, Initial Reports*, vol. 127. College Station, TX: Ocean Drilling Program, 323-412.
- Shipboard Scientific Party, 1990b. Site 798. In: Ingle, J.C., Jr., Suyehiro, K., von Breyman, M.T., et al. (eds.) *Proceedings of the Ocean Drilling Program, Initial Reports*, vol. 128. College Station, TX: Ocean Drilling Program, 121-216.
- Stuiver, M., Braziunas, T.F., Becker, B., Kromer, B., 1991. Climatic, solar, oceanic, and geomagnetic influences on late-glacial and Holocene atmospheric $^{14}\text{C}/^{12}\text{C}$ change. *Quaternary Research* 35, 1-24.
- Torrence, C., Compo, G.P., 1998. A practical guide to wavelet analysis. *Bull. Amer. Meteorol. Soc.*, 79, 61-78.
- Yamamoto, M., Oba, T., Shimamune, J., Ueshima, T., 2004. Orbital-scale anti-phase variation of sea surface temperature in mid-latitude North Pacific margin during the last 145,000 years. *Geophys. Res. Lett.* 31, L16311, doi:10.1029/2004GL020138.
- Yamamoto, M., Suemune, R., Oba, T., 2005. Equatorialward shift of the subarctic boundary in the northwestern Pacific during the last deglaciation. *Geophys. Res. Lett.* 32, L05609, doi:10.1029/2004GL021903.

Explanation of Figures and Tables

Figure 1 Map showing the location (black star) of four DSDP-ODP holes used in this paper. Black circles are the locations of piston cores used in previous papers around the Japanese Islands. 1: MD01-2421 (Koizumi et al., 2004; Koizumi and Yamamoto, 2010). 2: ODP Hole 1150A, and 3: ODP Hole 1151C (Koizumi and Sakamoto, 2003; Koizumi and Yamamoto, 2010). 4: DGC-6, 5: KH-86-2-9, 6: KH-84-3-33, 7: KH-84-3-9, 8: MD01-2409, and 9: MR97-04-1 (Koizumi et al., 2006). 10: POI-J3 and 11: CGC-8 (Koizumi, 2008). 12: MR02-03-2, 13: MR99-04-3, 14: MR00-05-2, and 15: MR99-04-2 (Koizumi and Yamamoto, 2010). 16: MD01-2407, 17: MD01-2408, and 18: KT94-15-5 (Koizumi and Yamamoto, 2011).

Figure 2 Sedimentation rates (sub-bottom depth-mcd versus sediment age-Ma curves based on chronostratigraphic framework (x) for three Sites in Table 3. Symbols on each accumulation curves indicate sampling points (Table 4-6 appendix).

Figure 3 Map showing the location of four DSDP-ODP cores (black circles), annual sea-surface temperatures ($^{\circ}\text{C}$), generalized distribution of surface water currents, and surface water-masses (Senjyu, 1999; Masujima et al., 2003). TSS: Tsushima Strait, TGS: Tsugaru Strait, SS: Soya Strait, MS: Mamiya Strait, TWC: Tsushima Warm Current, LC: Liman Current, EKWC: East Korean Warm Current, NKCC: North Korean Cold Current.

Figure 4 Compositions of *Twt* and comparison of annual sea-surface temperatures (SST) records between *Twt* and *Td'*-derived SST ($^{\circ}\text{C}$) at Site 436. The occurrences of characteristic warm- and cold-water taxa of *Twt* are indicated. Arrows indicate diatom datum levels. Vertical dashed-dotted lines represent the present-day values.

Figure 5 Stratigraphic variation of diatom abundance ($10^7/\text{g}$), relative abundance (%) of sublittoral taxa, compositions of *Twt* and *Td'*, and comparison *Twt* and *Td'*-derived SSTs ($^{\circ}\text{C}$) at Hole 797B. Vertical broken line (0.214 at diatom abundance- $10^7/\text{g}$) indicates the levels of samples under 100 diatoms in a relative abundance of 200 diatoms. Vertical dashed-dotted lines indicate the present-day values.

Figure 6 Stratigraphic variation of diatom abundance ($10^7/\text{g}$), relative abundance (%) of sublittoral taxa, comparison of warm- and cold-water taxa of *Td'*, and *Td'*-derived SSTs ($^{\circ}\text{C}$) at Holes 798A and C. Vertical dashed-dotted lines indicate the present-day values.

Figure 7 The wavelet analysis for the values of the band ration annual *Td'*-derived SST ($^{\circ}\text{C}$) at Site 798. a.: *Td'*- SST ($^{\circ}\text{C}$). b.: The wavelet power spectrum. The contour levels are chosen so that 75%, 50%, 25%, and 5% of the wavelet power is above each level, respectively. The cross-hatched region is the cone of influence, where zero padding has reduced the variance. Solid black contour indicates the 10 % confidence level, using a red-noise (autoregressive lag 1) background spectrum. c.: The global wavelet power

spectrum (black line). The dashed line is the significance for the global wavelet spectrum, assuming the same significance level and background spectrum as in b. Reference: Torrence, C. and G. P. Compo, 1998: A Practical Guide to Wavelet Analysis. Bull. Amer. Meteor. Soc., 79, 61-78.

Table 1 Species composition for Td' (Koizumi, 2008).

Table 2 Species composition for Twt $[=(Xw+0.5Xt)/(Xc+Xt+Xw)]$. Xw : the total percentage of tropical-tropical (warm-water) taxa, Xt : the total percentage of warm-water transitional taxa, Xc : the total percentage of subarctic (cold-water) taxa.

Table 3 Chronostratigraphic framework (depth vs. calendar age) in three cores used in this study. LC: last common occurrence, L: last occurrence, B: base, T: top.

Table 4 appendix The occurrences of diatoms in Site 436.

Table 5 appendix The distribution of diatom abundance ($10^7/g$) and occurrence of diatoms in Hole 797B.

Table 6 appendix The distribution of diatom abundance ($10^7/g$) and occurrence of diatoms in Holes 798A and C.

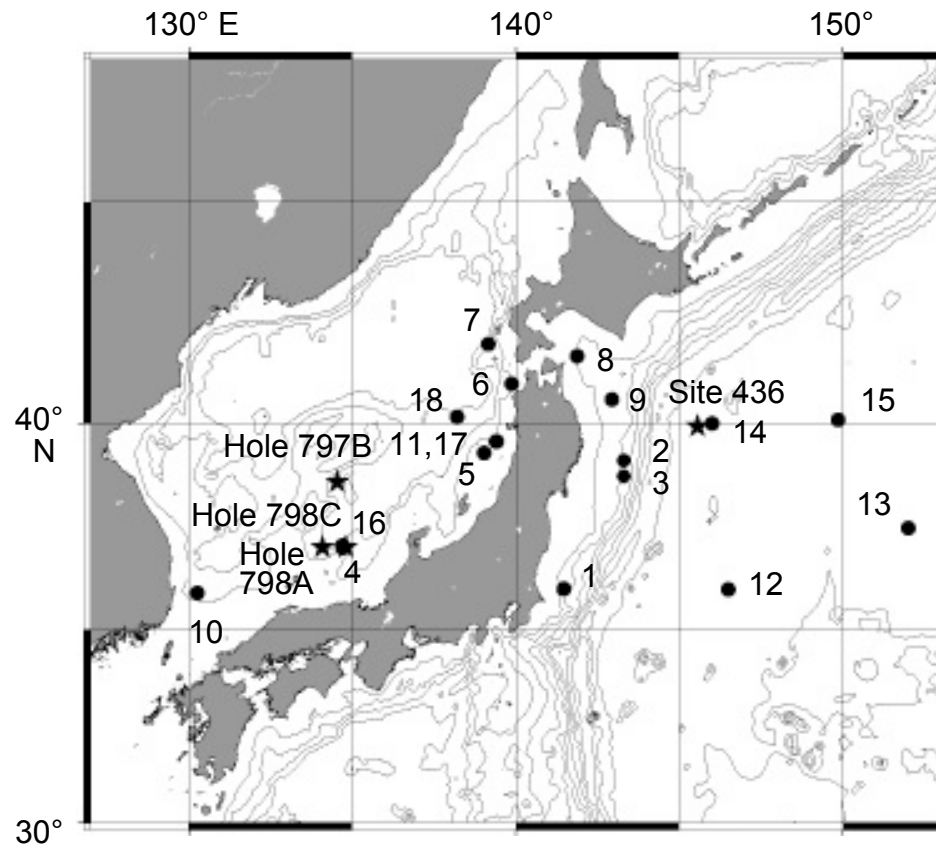


Figure 1

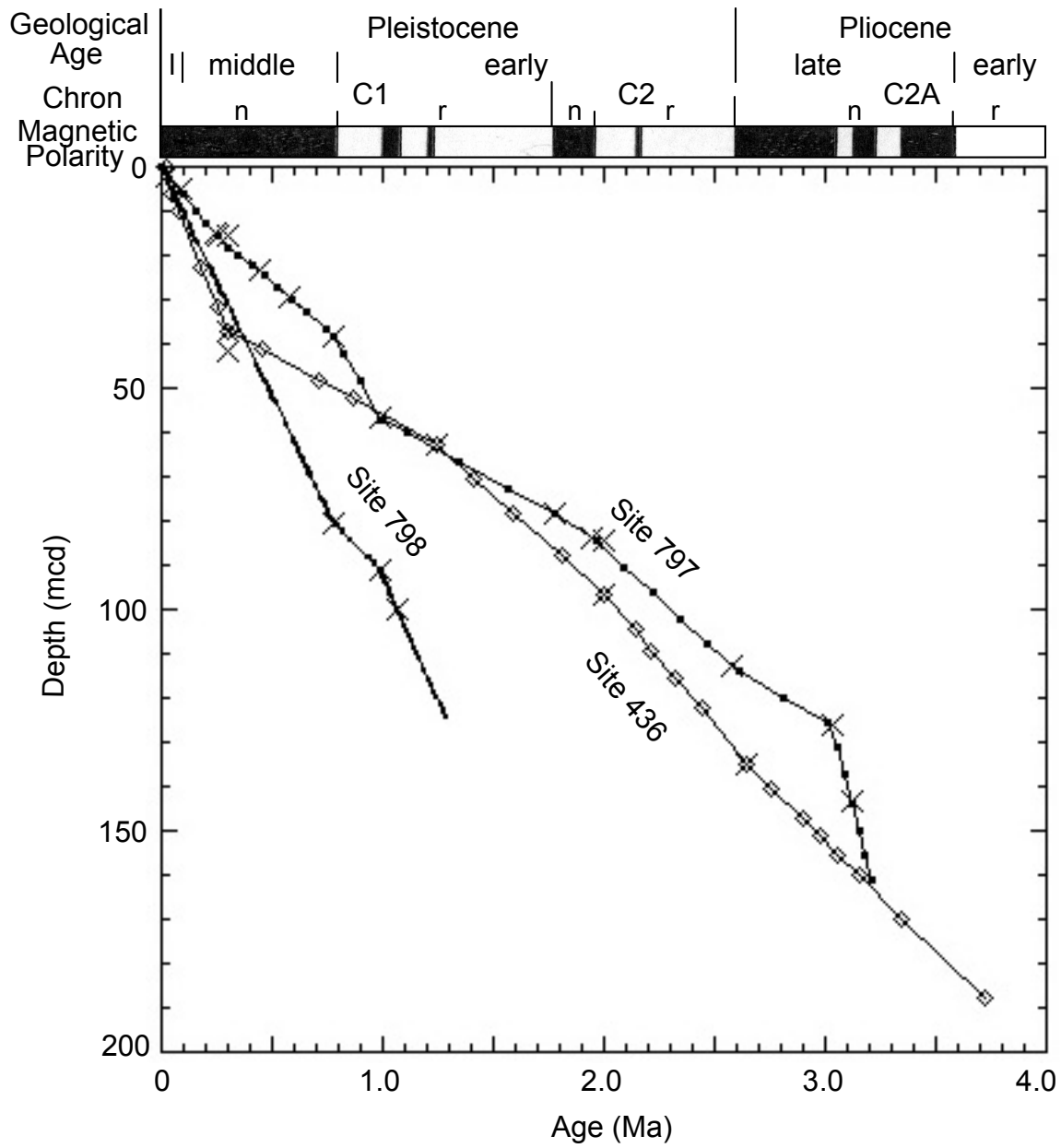


Figure 2

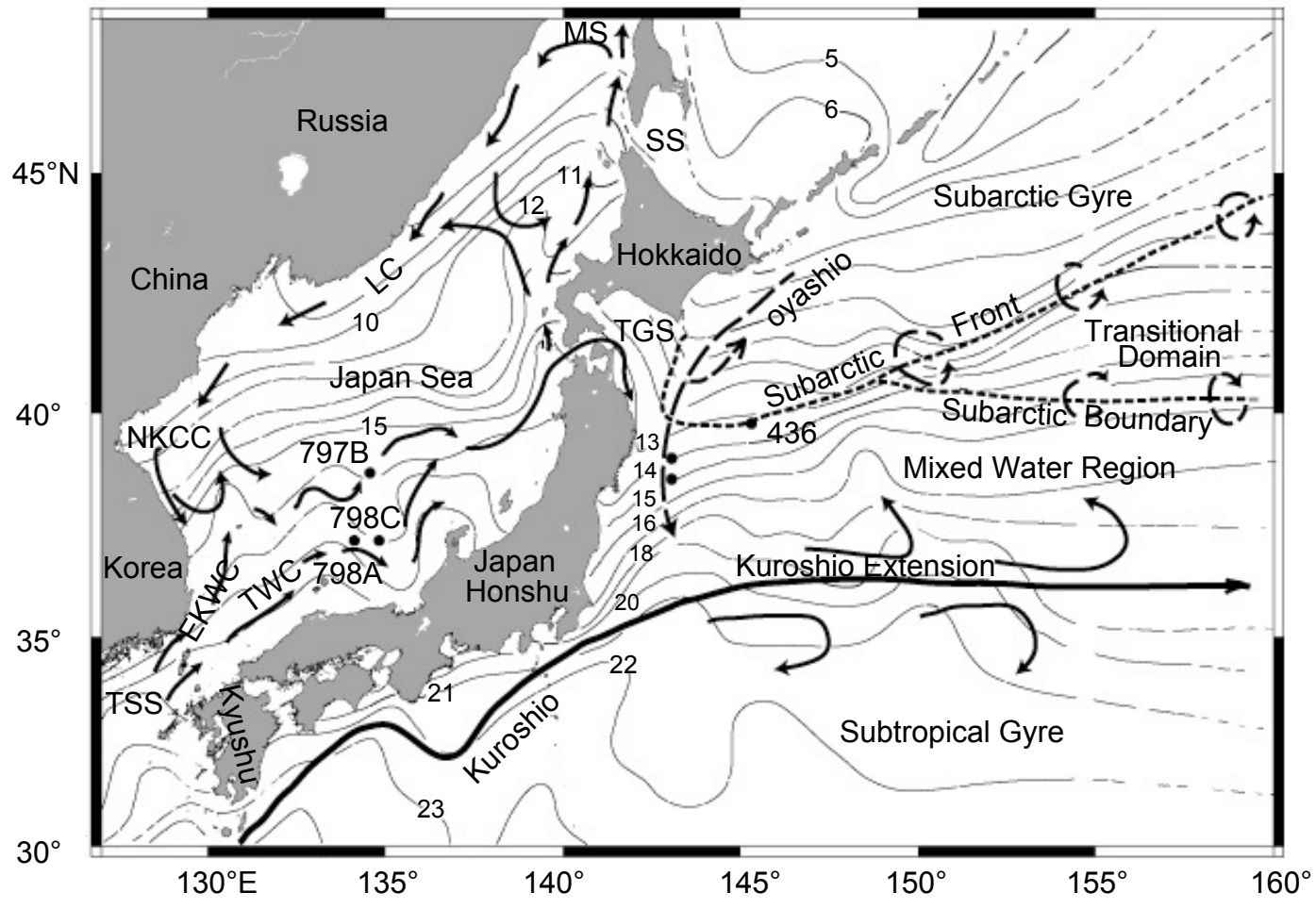


Figure 3

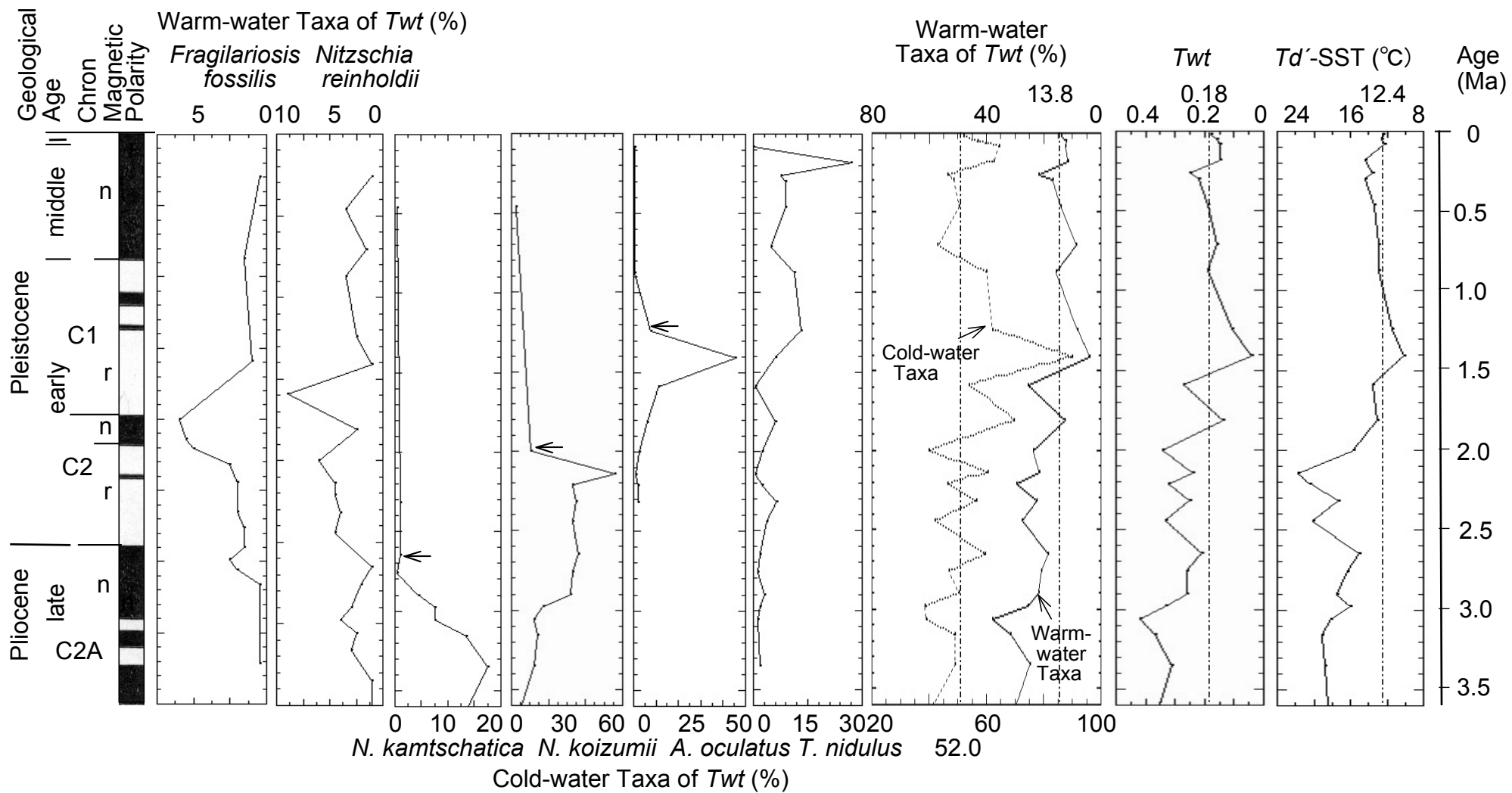


Figure 4

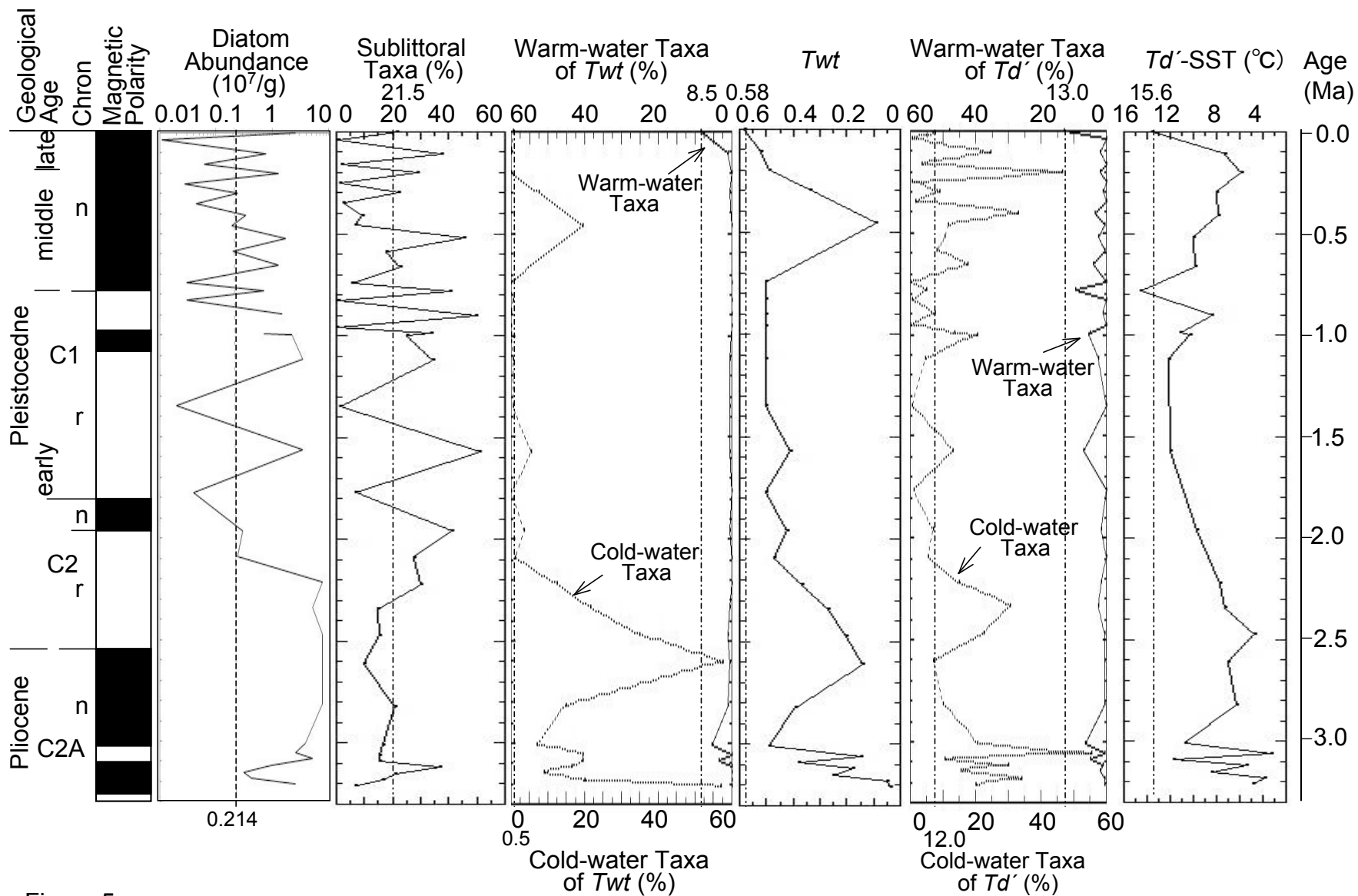


Figure 5

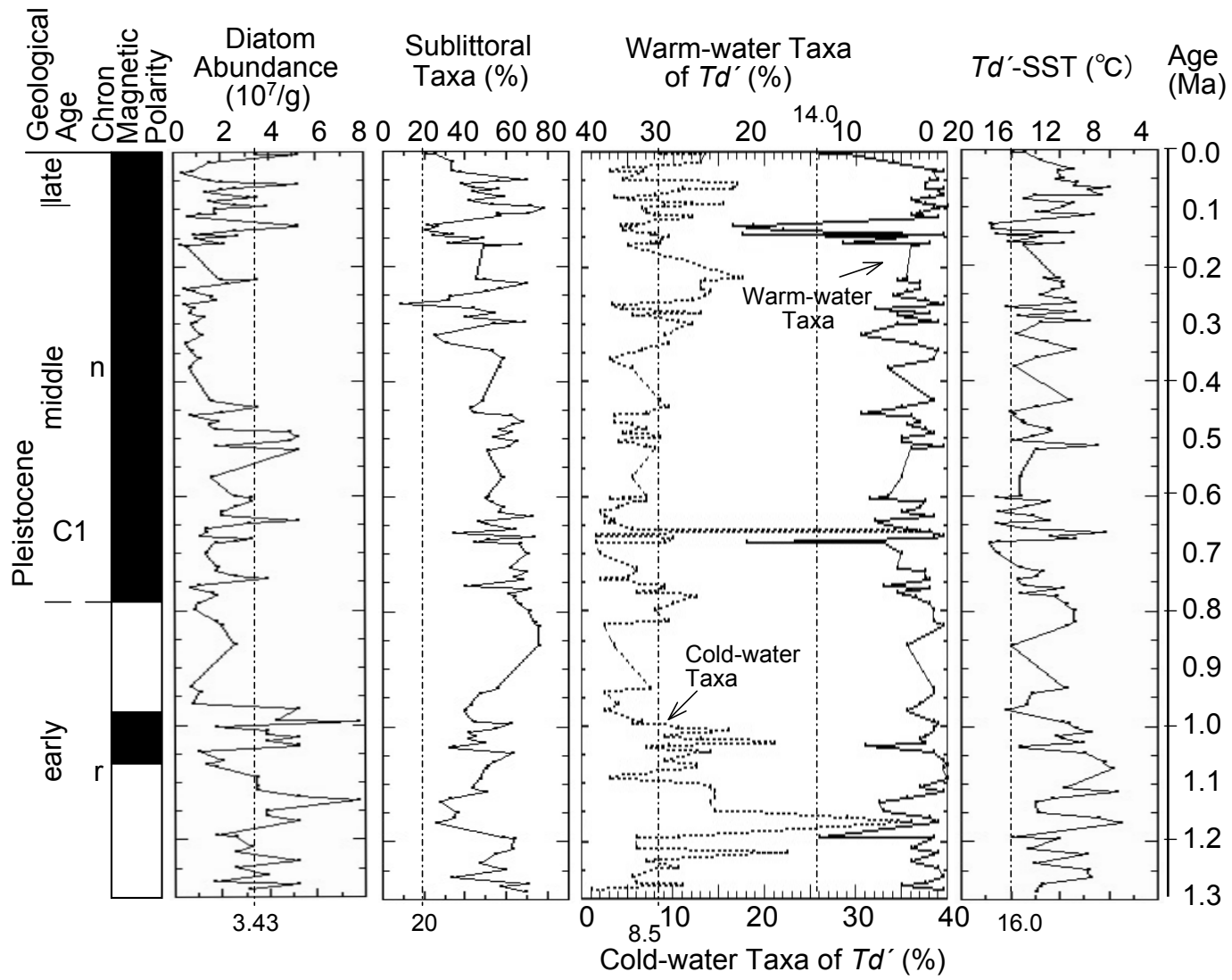


Figure 6

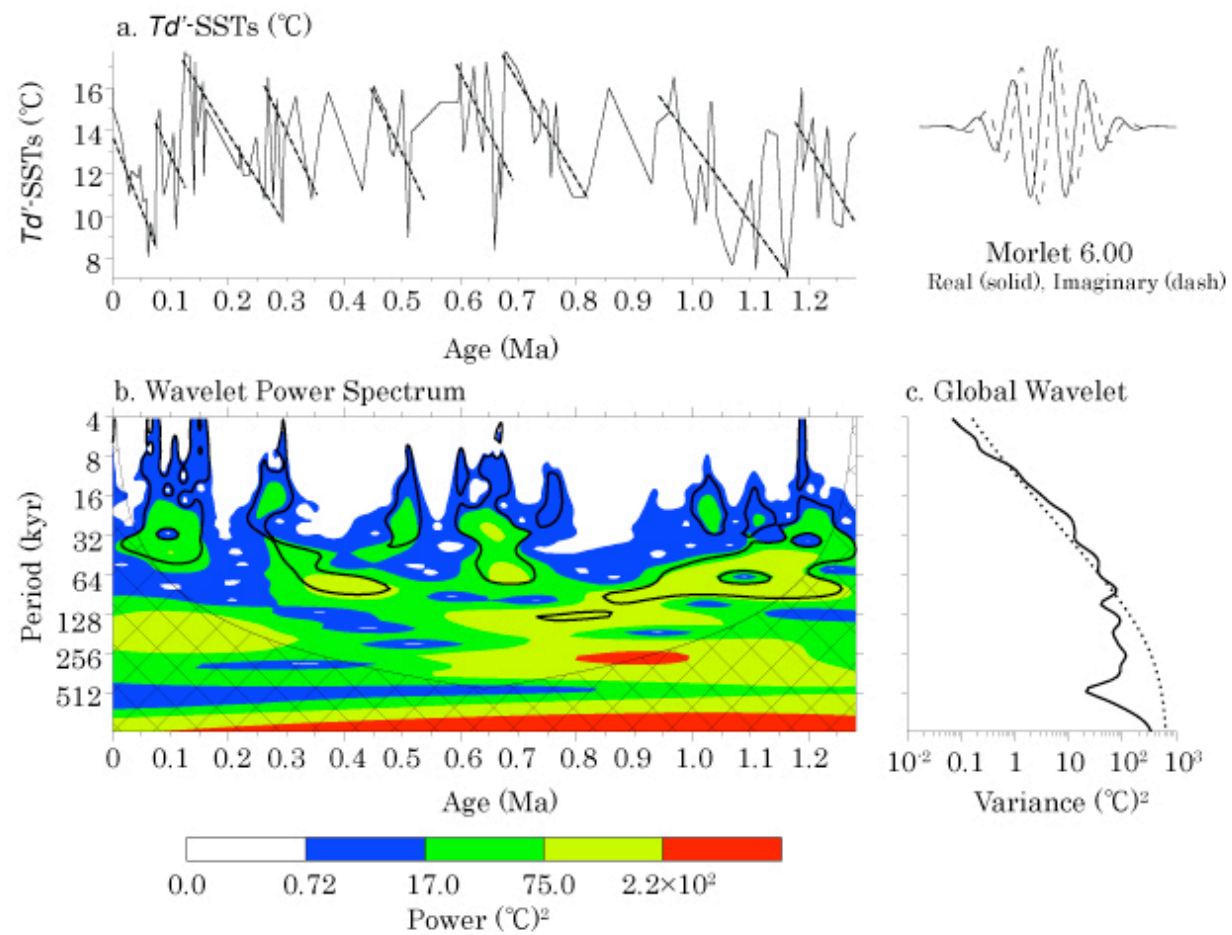


Figure 7 for online

Table 1

<i>Td'</i>	
Warm-water species	Cold-water species
<i>Actinocyclus ellipticus</i> Grunow	<i>Actinocyclus curvatulus</i> Janisch
<i>A. elongatus</i> Grunow	<i>A. ochotensis</i> Jousé
<i>Alveus marinus</i> (Grunow) Kaczmarek & Fryxell	<i>Asteromphalus hyalinus</i> Karsten
<i>Asterolampra marylandica</i> Ehrenberg	<i>A. robustus</i> Castracane
<i>Asteromphalus arachne</i> (Brebisson) Ralfs	<i>Bacterosira fragilis</i> Gran
<i>A. flabellatus</i> (Brebisson) Greville	<i>Chaetoceros furcellatus</i> Bailey
<i>A. imbricatus</i> Wallich	<i>Coscinodiscus marginatus</i> Ehrenberg
<i>A. petterssonii</i> (Kolbe) Thorrington-Smith	<i>C. oculus-iridis</i> Ehrenberg
<i>A. sarcophagus</i> Wallich	<i>Fragilariopsis cylindrus</i> (Grunow) Krieger
<i>Azpeitia africanus</i> (Janisch) Fryxell & Watkins	<i>F. oceanica</i> (Cleve) Hasle
<i>A. nodulifera</i> (Schmidt) Fryxell & Sims	<i>Neodenticula seminae</i> (Simonsen & Kanaya) Akiba & Yanagisawa
<i>A. tabularis</i> (Grunow) Fryxell & Sims	<i>Porosira glacilis</i> (Grunow) Jorgensen
<i>Fragilariopsis doliolus</i> (Wallich) Medlin & Sims	<i>Rhizosolenia hebetata</i> (Bailey) Gran
<i>Hemidiscus cuneiformis</i> Wallich	<i>Thalassiosira gravida</i> Cleve
<i>Nitzschia interruptestriata</i> Simonsen	<i>T. hyalina</i> (Grunow) Gran
<i>N. kolaczekii</i> Grunow	<i>T. kryophila</i> (Grunow) Joergensen
<i>Planktoniella sol</i> (Wallich) Schütt	<i>T. nordenskioldii</i> Cleve
<i>Pseudosolenia calcar-avis</i> (Schültze) Sundstrom	<i>T. trifulta</i> Fryxell
<i>Rhizosolenia acuminata</i> (Peragallo) Gran	
<i>R. bergonii</i> Peragallo	
<i>R. hebetata</i> (Bailey) Gran f. <i>semispina</i> (Hersen) Gran	
<i>R. imbricata</i> Brightwell	
<i>Roperia tessellata</i> (Roper) Grunow	
<i>Thalassiosira leptopus</i> (Grunow) Hasle & Fryxell	
<i>T. oestrupii</i> (Osterfeld) Proshkina-Lavrenko	

Table 2

<i>Twt</i>	
<i>Xw</i> of <i>Twt</i>	<i>Xt</i> of <i>Twt</i>
Warm-water species without <i>T. oestrupii</i> of <i>Td'</i> <i>Fragilariopsis fossilis</i> (Frenguelli) Medlin & Sims <i>F. reinholdii</i> (Kanaya emend Barron & Baldauf) Zielinski & Gersonde <i>Nitzschia jouseae</i> Burckle <i>N. miocenica</i> Burckle <i>Rhizosolenia praebergonii</i> Mukhina <i>Thalassiosira convexa</i> Mukhina <i>T. miocenica</i> Schrader <i>T. praecovexa</i> Burckle	<i>Coscinodiscus radiatus</i> Ehrenberg <i>Thalassionema nitzschioides</i> Grunow s.l. <i>Thalassiosira oestrupii</i> (Osterfeld) Proshkina-Lavrenko

Xc of Twt

Cold-water species of *Td'*

Actinocyclus oculatus Jousé

Neodenticula kamtschatica (Zabelina) Akiba & Yanagisawa

N. koizumii Akiba & Yanagisawa

Proboscia barboi (Brun) Jordan & Priddle

P. curvirostris (Jousé) Jordan & Priddle

Thalassiosira nidulus (Tempère & Brun) Jousé

Table 3

Age Controls	Age (Ma)	Sub-bottom Depth (mcd)		
		Site 436	Hole 797B	Holes 798A and C
AT tephra	0.024		2.24	
Aso-4 tephra	0.088		5.21	
Ata-Th tephra	0.244		15.22	
L <i>Proboscia curvirostris</i>	0.30	37.10	15.57	41.85
Aso-1 tephra	0.255		15.66	
B-Og tephra	0.447		23.58	
Baegdusan tephra	0.580		29.46	
B C1n (B Brunhes)	0.78		38.30	80.5
T C1r.1n (T Jaramillo)	0.99		56.64	91.0
B C1r.1n (B Jaramillo)	1.07			100.0
LC <i>Actinocyclus oculatus</i>	1.24	62.60		
T C2n (T Olduvai)	1.78		78.43	
B C2n (B Olduvai)	1.95		83.90	
L <i>Neodenticula koizumii</i>	2.00	96.70	84.5	
T C2An (T Gauss)	2.58		113.00	
LC <i>Neodenticula kamtschatica</i>	2.65	135.00		
T C2An.1r (T Kaena)	3.03		126.00	
B C2An.1r (B Kaena)	3.12		143.50	

Table 5

Depth (m)	0.13	2.75	6.33	9.79	12.69	15.55	18.45	20.20	22.22	24.27	26.99	29.78	32.81	35.57	38.29	42.42	48.35	56.97	57.52	60.09	65.52	74.54	78.28	84.40	90.49	96.33	101.99	107.99	113.79	119.79	126.47	131.29	137.49	143.79	150.03	155.66	161.29				
Age (Mo)	0.001	0.035	0.108	0.159	0.205	0.252	0.300	0.350	0.408	0.463	0.524	0.587	0.656	0.741	0.800	0.827	0.895	0.994	1.000	1.115	1.248	1.567	1.775	1.863	2.093	2.219	2.342	2.472	2.607	2.815	3.012	3.057	3.088	3.122	3.154	3.183	3.212				
Abundance (1007/a)	2.97	0.91	0.77	0.98	1.29	0.93	0.24	0.04	0.24	0.19	1.71	0.20	1.29	0.93	0.70	0.63	1.47	0.70	2.20	3.43	0.92	3.43	0.04	0.20	0.24	7.71	5.14	7.71	7.71	7.71	3.88	2.97	5.14	0.96	0.31	0.43	2.97				
<i>Alexis marina</i>	1																																								
<i>Asteromphalus fabelatus</i>	1																																								
<i>Aspeitha nodifera</i>	3																																								
<i>A. tabularia</i>	4																																								
<i>Coscinodiscus perforatus</i>	3																																								
<i>Fragilaropsis delioles</i>	6	2																																							
<i>Hemidiscus cuneiformis</i>	1																																								
<i>Mitochondria kobczeki</i>	1																																								
<i>Rhizosolenia begoii</i>	1																																								
<i>R. imbricata</i>	2																																								
<i>Rapheia tessellata</i>	1																																								
<i>T. ostrucii</i>	9	2	4	1	4	1	5	1	8	5	2	10	9	5	13	2	3	4	1	1	1	1	1	1	1	1	1	1	1	1	1	1	1	1	1	1	1	1	1	1	
Warm water species of <i>T. ostrucii</i>	27	4	4	3	7	1	5	1	8	19	2	10	11	5	14	3	3	5	1	1	1	1	1	1	1	1	1	1	1	1	1	1	1	1	1	1	1	1	1	1	
<i>Actinocyclus curvatus</i>	3	1	1	3	1	35	2	4	2	2																															
<i>A. subtenis</i>	1																																								
<i>Asteromphalus robustus</i>	1																																								
<i>Bacterosira fragilis</i>	1																																								
<i>Chaetoceros furcellatus</i>	1																																								
<i>Coscinodiscus marginatus</i>	12	1	5	5	3	1	3	1	10	11																															
<i>C. oculum-vidis</i>	8																																								
<i>Neodenticula seminiae</i>	3	6	12																																						
<i>Parasira glacialis</i>	1																																								
<i>Rhizosolenia hebetata</i>	23	2	63																																						
<i>Thalassiosira gravida</i>	1																																								
<i>T. nordenskiöldii</i>	1																																								
<i>T. triifida</i>	4	13	13																																						
Cold water species of <i>T. ostrucii</i>	25	1	51	7	93	1	18	3	66	23	21	16	35	10	1	15	27	41	9	1	26	2	14	11	30	61	45	14	20	41	111	21	60	31	88	40					
<i>T. ostrucii</i>	0.52	0.00	0.07	0.00	0.04	0.00	0.14	0.00	0.10	0.42	0.19	0.08	0.19	0.00	0.88	0.00	0.12	0.27	0.21	35.20	0.00	35.00	0.00	17.60	0.00	8.10	7.60	2.20	6.70	4.80	24.10	0.50	32.30	3.00	11.40	1.40	2.40				
Warm water species without <i>T. ostrucii</i> of <i>T. ostrucii</i>	18	2																																							
<i>Fragilaropsis reinholdi</i>	1																																								
<i>Thalassiosira convexa</i>	1																																								
<i>X. of <i>T. ostrucii</i></i>	18	2																																							
<i>Coscinodiscus radiatus</i>	12	4																																							
<i>Thalassiosira nitrochlorides</i>	61	1	47	2	41	1	22	2	24	7	12	10	2	3	51	1	73	56	47	99	3	33	2	28	32	70	47	42	41	100	91	16	88	17	14	3	9				
<i>Thalassiosira oestrupii</i>	9	2	4																																						
<i>X. of <i>T. ostrucii</i></i>	82	1	53	2	45	1	27	2	31	8	17	11	10	3	60	1	75	66	56	104	3	45	2	28	32	73	51	43	42	101	53	17	92	19	18	4	10				
Cold water species of <i>T. ostrucii</i>	25	1	51	7	93	1	18	3	66	23	21	16	35	10	1	15	27	41	9	1	26	2	14	11	30	61	45	14	20	41	111	21	60	31	88	40					
<i>Actinocyclus oculatus</i>	1																																								
<i>Neodenticula kamtschatica</i>	1																																								
<i>N. koizumi</i>	1																																								
<i>Robococca barboi</i>	1																																								
<i>P. curvirostris</i>	1																																								
<i>Thalassiosira radialis</i>	1																																								
<i>X. of <i>T. ostrucii</i></i>	25	1	51	7	93	4	33	6	70	59	71	24	39	23	2	15	43	57	1	1	11	0	7	2	25	43	70	115	30	14	39	39	33	18	40	114					
<i>T. ostrucii</i>	0.58	0.00	0.92	0.00	0.49	0.00	0.34	0.00	0.00	0.09	0.00																														

117.0	119.0	120.0	121.7	123.0	123.3	124.3
904.9	921.2	950.1	962.3	992.9	1000.0	1023.7
2.57	5.14	2.57	3.86	1.63	5.14	3.09

2

1 1

1

2 1 1

1 1 1 1 4 3

1	4	1	4	3
---	---	---	---	---

2	8	2	1	5	10
---	---	---	---	---	----

1 1 1 5 1

1 1

3 3 1 3 1 2

1 1 1 1 1 7

33 7 17 6 4 5

1 1

7 1 3

2 2

45	14	21	11	12	22
----	----	----	----	----	----

94	264	87	83	294	313
----	-----	----	----	-----	-----

99	142	97	95	134	136
----	-----	----	----	-----	-----

2

2

3 1 1

1 1 1 1 2

1

37 63 49 116 35 32 49

2 1 2 7 4

3 1 3 1 2 7 4

2 1 2 3 1

4 2 1

2	9	3	1	3
---	---	---	---	---

44	84	98	121	39	53
----	----	----	-----	----	----

13	10	4	10	5	1
----	----	---	----	---	---

11	20	10	4	5	7
----	----	----	---	---	---

2 7 20

9 7 3 6 2 8 3

1 1 3 1 1 2

1 2 1 1 1 1 2

11 7 21 5 22 15 15

1 3 1 2 1 5

30 24 24 18 50 39 61

17 10 38 14 47 34 11

4 1 1 1 1

108	93	118	67	139	114
-----	----	-----	----	-----	-----

1

						1
1	1	1		2		
			3		1	
1	1	1		5	1	
200	200	200	200	200	200	200